

PAPER • OPEN ACCESS

## Impact parameter selective Rydberg atom collision by optical tweezers

To cite this article: Hansub Hwang *et al* 2025 *J. Phys. B: At. Mol. Opt. Phys.* **58** 115202

View the [article online](#) for updates and enhancements.

You may also like

- [A revisit on linear wavepacket interferometry with phase-locked pulse pairs: spatiotemporal dynamics and evolution of information entropy](#)  
Subho Mitra and Arijit K De
- [Strongly confined atomic excitation localization in a weakly-driven atom-waveguide interface](#)  
Shao-Hung Chung, Wei Chen and H H Jen
- [Photoionization of the O<sub>2</sub> molecule](#)  
M C Zammit, J P Colgan, C J Fontes et al.

# Impact parameter selective Rydberg atom collision by optical tweezers

Hansub Hwang<sup>1,3</sup> , Sunhwa Hwang<sup>1</sup> , Jaewook Ahn<sup>1</sup> , Shuhei Yoshida<sup>2,\*</sup>   
and Joachim Burgdörfer<sup>2</sup> 

<sup>1</sup> Department of Physics, KAIST, Daejeon 34141, Republic of Korea

<sup>2</sup> Institute for Theoretical Physics, Vienna University of Technology (TU Wien), Vienna, EU, Austria

E-mail: [shuhei@concord.itp.tuwien.ac.at](mailto:shuhei@concord.itp.tuwien.ac.at)

Received 14 March 2025, revised 29 April 2025

Accepted for publication 20 May 2025

Published 30 May 2025



CrossMark

## Abstract

Optical tweezers are used to facilitate cold collisions between two Rydberg rubidium atoms ( $^{87}\text{Rb}$ ) by controlling the impact parameter and collision energy. One atom is held stationary while the other is propelled to a constant velocity. After the tweezers are deactivated, both atoms are excited to a Rydberg state using a  $\pi$ -pulse. Following the collision, a second  $\pi$ -pulse is applied. If the stationary atom undergoes minimal momentum transfer and returns to its ground state, it can be recaptured when the tweezer is reactivated. The collision probability as a function of the impact parameter is extracted from the atom loss in the tweezer and used to determine the collisional cross section between Rydberg atoms. Numerical simulations of elastic two-body collisions agree well with the experimental data, providing valuable insights into the parameter regime where quantum effects will become important.

Keywords: Rydberg atom, elastic collision, optical tweezer

## 1. Introduction

Optical tweezers are tightly focused beams of light used to trap and manipulate microscopic or submicroscopic particles, enabling numerous applications across various scientific and technological fields, including biology, quantum optics, optomechanics, atomic physics, and, more recently, quantum technologies [1–7]. A recent study has introduced a novel use of optical tweezers: accelerating neutral, single atoms [8]. Directly accelerating neutral particles has long been an experimental challenge, as conventional particle accelerators operate on charged particles. Creating a neutral particle beam typically

requires a neutralization step, which restricts the range of accessible projectiles, achievable energies, and beam focusing capabilities [9, 10]. Optical tweezers, however, present a promising approach to neutral particle acceleration, potentially opening new avenues for studying atomic and molecular collisions in previously inaccessible regimes. In comparison to optical lattice conveyor belts which can be employed to accelerate a thermal cloud of atoms [11], optical tweezers can reach larger accelerations of a single atom.

Low-energy collision studies often rely on low-temperature gases [12–15], which can make it difficult to perform controlled experiments, especially for molecular collisions [16]. A technique that precisely controls cold collisions at the single-atom level could facilitate investigations involving a specific number of particles rather than ensembles, and enable studies in arbitrary collision geometries. Such capabilities offer deeper insights into the fundamental nature of these interactions [17–19].

In this paper, we focus on using optical tweezers to facilitate low-energy collisions between two Rydberg atoms [10, 20–25]. Optical tweezers are employed to accelerate a single rubidium ( $^{87}\text{Rb}$ ) atom and allow to observe the pairwise

<sup>3</sup> Current address: The Department of Physics, University of Wisconsin Madison, Madison, WI 53706, United States of America

\* Author to whom any correspondence should be addressed.



Original Content from this work may be used under the terms of the [Creative Commons Attribution 4.0 licence](https://creativecommons.org/licenses/by/4.0/). Any further distribution of this work must maintain attribution to the author(s) and the title of the work, journal citation and DOI.

collision between two Rydberg-state atoms by controlling the collision velocity and the impact parameter. Moreover, optical tweezers provide a new probing scheme for elastic scattering by measuring the momentum transfer to atoms. This differs from typical probing schemes used for inelastic Rydberg-atom collisions, for which the effects of collisions are quantified as a change in electronic excitation through inelastic scattering by measuring ionization or field-ionization after collisions [21, 22, 24, 27, 28].

The experimental procedure of the Rydberg-atom collision experiment is depicted in figure 1. The projectile rubidium atom (labeled as *A*), initially in the ground state  $|g\rangle = |5S_{1/2}, F=2, m_F=2\rangle$  (shown in blue), is accelerated by a dynamic optical tweezer and thrown at the target atom with velocity  $v$ . Both atoms, the projectile atom *A* and the target atom *B*, are then optically excited to the Rydberg state,  $|n\rangle = |nS_{1/2}, F=2, m_F=2\rangle$  (shown in red), prior to the collision. After the collision, atom *B* is de-excited back to  $|g\rangle$  and may be recaptured by another optical tweezer. This recapture probability,  $P_B(b; n, v)$ , for atom *B* to survive the collision and to be recaptured, is measured as a function of the impact parameter  $b$ , the relative velocity  $v$ , and the principal quantum number  $n$ . The collisional cross section is then determined from this recapture probability.

The paper is organized as follows: section 2 describes the experimental setup and procedure. In section 3, we discuss the theory of Rydberg–Rydberg collisions. Experimental results are presented in section 4, followed by their discussion in section 5. Conclusions are given in section 6.

## 2. Experimental procedure

The experimental setup encompasses a system with a magneto-optical trap for cooling  $^{87}\text{Rb}$  atoms, an optical tweezer configuration consisting of both static and dynamic tweezers, and an imaging system for analyzing collision events [29–32]. In the initial phase of the experiment, two rubidium atoms, cooled to  $30\ \mu\text{K}$  in the MOT, are selected from specific locations. Atom *A* is positioned at coordinates  $(x_A = b, 0, -z_A)$ , while atom *B* is at  $(0, 0, 0)$ . This selection process is performed using static optical tweezers, controlled by a two-dimensional (2D) spatial light modulator (SLM, ODPDM-512 from Meadowlark Optics). Next, a dynamic optical tweezer is gradually activated to capture atom *A*. The dynamic tweezer is controlled by a 2D acoustic-optic modulator (AOD, DTSxy-400-820 from AA Opto Electronics) and an arbitrary waveform generator (AWG, M4i-6622-x8 from SPECTRUM Instrument,  $625\ \text{MS}^{-1}$ ). The optical potentials and beam widths of the static and dynamic tweezers are  $U_s = 0.58(5)\ \text{mK}$ ,  $U_d = 10(1)\ \text{mK}$ ,  $d_s = 0.79(4)\ \mu\text{m}$ , and  $d_d = 0.75(4)\ \mu\text{m}$ , respectively, corresponding to trap frequencies of  $\omega_s/(2\pi) = 67(6)\ \text{kHz}$  and  $\omega_d/(2\pi) = 294(30)\ \text{kHz}$ . The optical parameters are governed by system-specific factors, including lens NA, available laser power, and the response time of the AOD [33].

The next step involves accelerating atom *A* along the  $z$ -axis to a constant velocity in free flight [8]. This motion is initiated by applying a constant acceleration  $\ddot{z} = a$  to the dynamic optical tweezer. The tweezer is deactivated at  $t=0$  when the position  $z = -z_i$  is reached, thereby releasing atom *A* with a velocity  $v$ . In this experiment, the tweezer is either accelerated at  $2.8(4) \times 10^5\ \text{m s}^{-2}$  over a duration of  $10.6(8)\ \mu\text{s}$  and a traveling distance of  $15.9(3)\ \mu\text{m}$  to reach the final velocity  $v = v_{\text{fast}} = 3.0(2)\ \text{m s}^{-2}$  or at  $0.8(1) \times 10^5\ \text{m s}^{-2}$  over a duration of  $10.6(8)\ \mu\text{s}$  and a distance of  $4.5(3)\ \mu\text{m}$  to reach the final velocity  $v = v_{\text{slow}} = 0.85(9)\ \text{m s}^{-2}$ . Simultaneously, the static optical tweezers are deactivated, releasing the stationary atom *B*. Just before release, the temperatures of atoms *A* and *B*, while confined in the optical tweezers, were  $T_A = 150(20)\ \mu\text{K}$  and  $T_B = 30(4)\ \mu\text{K}$ , respectively. The higher temperature of atom *A* is attributed to the adiabatic increase in trap depth before acceleration [34]. These temperatures result in position broadenings of  $0.06\ \mu\text{m}$  for atom *A* and  $0.13\ \mu\text{m}$  for atom *B*, with corresponding velocity broadenings of  $\Delta v = 0.12\ \text{m s}^{-2}$  for atom *A* centered about  $v$  and  $\Delta v = 0.05\ \text{m s}^{-2}$  for atom *B* centered about zero.

The third step in our experimental process involves excitation of the atoms to a Rydberg state before the collision and their subsequent de-excitation after the collision. Both atoms are excited to the same Rydberg state, chosen to be  $|36S_{1/2}\rangle$ ,  $|45S_{1/2}\rangle$ , or  $|53S_{1/2}\rangle$ , at  $t_1 \simeq 1\ \mu\text{s}$ . These particular Rydberg states are selected based on the constraints of our frequency-locking system, which uses a dual-frequency Fabry–Perot resonator (Stable Laser Systems, ATF-6010-4). To induce the two-photon transition from  $|g\rangle$  to the state  $|nS_{1/2}\rangle$  with a quantum defect  $\delta = 3.135$ , we use 780 nm and 480 nm lasers directed perpendicular to the atomic motion. The effective Rabi frequency for the Rydberg excitation is determined experimentally and described by:

$$\Omega(\vec{r}, t) = \Omega_0 e^{-\frac{x^2 + y^2 + (z - z_R)^2}{\sigma_R^2}} \Pi\left(\frac{t - t_{1,2}}{\pi/\Omega_0}\right), \quad (1)$$

where  $z_R = -4.5(3)\ \mu\text{m}$  and  $\sigma_R = 6.8(1)\ \mu\text{m}$  represent the center and width of the Rydberg excitation laser, and the peak Rabi frequency is  $\Omega_0/(2\pi) \simeq 1\ \text{MHz}$ , varying slightly depending on  $n$  and  $v$ . The function  $\Pi(x)$  is a rectangular function defined as  $\Pi(x) = 1$  for  $|x| < 1/2$  and 0 for  $|x| > 1/2$ .

After atom *A* passes by atom *B*, both are de-excited to their ground state at  $t_2 \simeq 7\ \mu\text{s}$  for  $v = v_{\text{fast}}$  and  $t_2 \simeq 32\ \mu\text{s}$  for  $v = v_{\text{slow}}$ . In the final step, at time  $t_f \simeq t_2 + 1.5\ \mu\text{s}$ , the static optical tweezer is reactivated at the original location where the atom *B* was initially positioned. This reactivation allows to determine whether the atom *B* is still present within the recapture zone, defined by a radius of  $d_B = d_s$  centered at  $(0, 0, 0)$ , where  $d_B$  serves as the effective boundary of our optical tweezer, approximated in terms of a truncated harmonic potential. A sequence of two  $\pi$ -pulses is applied to manipulate the electronic state of the atom at the center of the laser focus. To enhance the efficiency of de-exciting the atom *B* with the second  $\pi$ -pulse, a spin-echo protocol is employed, flipping

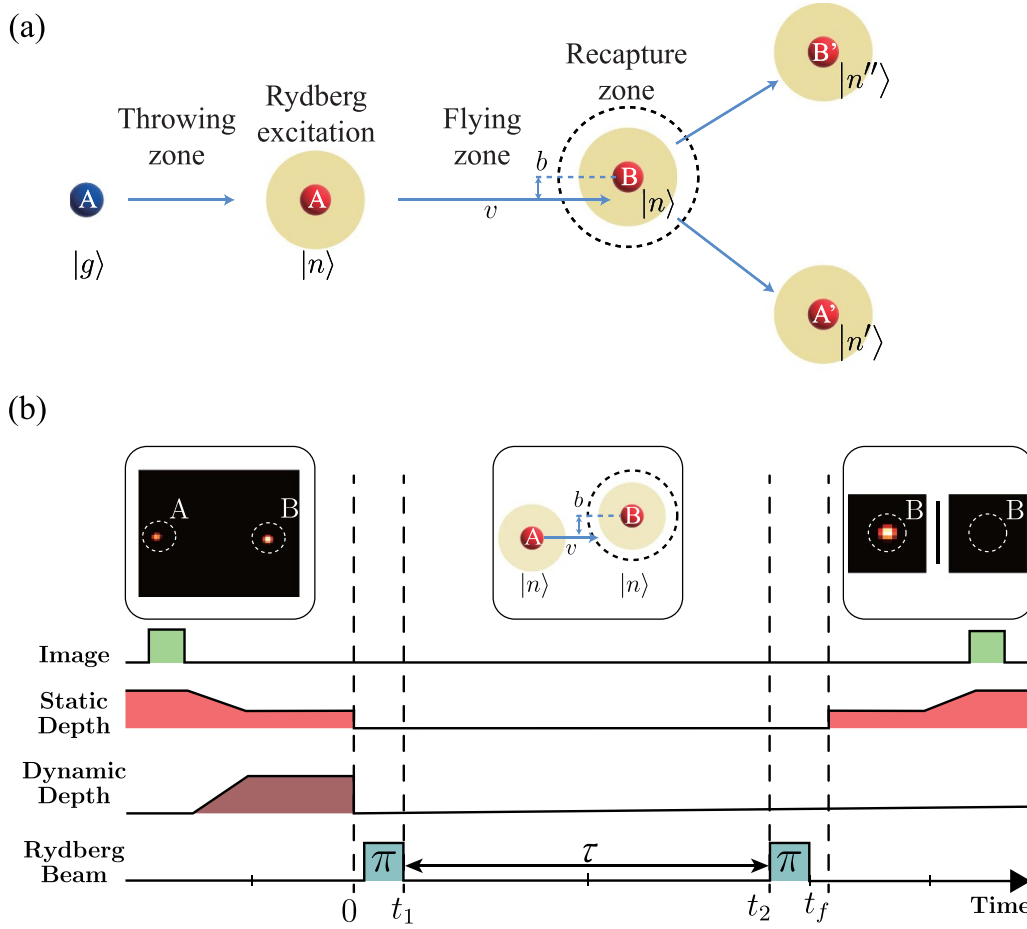


**Figure 1.** (a) Schematic of the Rydberg-atom collision experiment. (b) Experimental time sequence: initially, two atoms A and B are captured in static optical dipole traps from a cloud of  $^{87}\text{Rb}$  atoms. Once the atoms are successfully captured, atom A is gradually transported from the static trap to the dynamic trap for acceleration. Subsequently, atom A is propelled using the dynamic trap, and all dipole traps are deactivated. A Rydberg excitation beam is then introduced to facilitate Rydberg–Rydberg atom collisions. The experiment concludes by applying the Rydberg de-excitation beam and probing the recapture of atom B to detect the occurrence of Rydberg collisions.

the laser phase at the midpoint  $t = (t_1 + t_2)/2$ . For detection, fluorescence imaging is used, based on the cycling transition  $|5S_{1/2}\rangle \leftrightarrow |5P_{3/2}\rangle$ . This imaging is performed with an exposure time of over 50 ms, utilizing an electron-multiplying charge-coupled device (Ixon Ultra 897 from Andor) [36].

Due to the velocity spread  $\Delta v$  of the atom B at rest only on average, it may escape the recapture zone before the tweezer is reactivated, even without undergoing a collision. To account for this, we alternate measurements of atom B in the presence ( $P_B(x_A; n, v)$ ) and absence ( $P_B^{(0)}(n, v)$ ) of atom A. The true recapture probability is then extracted from

$$P_{\text{recap}}(x_A; n, v) = \frac{P_B(x_A; n, v)}{P_B^{(0)}(n, v)}. \quad (2)$$

Any additional atom loss can thus be attributed to collisions, and the corresponding collision probability can be defined as

$$P_{\text{coll}}(x_A; n, v) = 1 - P_{\text{recap}}(x_A; n, v). \quad (3)$$

This collision probability includes only ‘hard’ elastic collisions with momentum transfers large enough such that atom B will escape the tweezer irrespective of its initial position and

of its initial thermal velocity. The present experimental procedure is repeated about 1000 times to accumulate the data.

### 3. Collision between Rydberg atoms

We focus in this communication on elastic scattering between atoms, i.e. the collision energy is preserved without changing the electronic state of the atoms. In the present experiment the collision velocity is sufficiently low such that significant contributions from inelastic (de)excitation processes of the Rydberg electrons can be ruled out as the relative kinetic energy carried into the collision does not exceed the energy spacing between adjacent Rydberg manifolds. We have verified the predominantly quasi-elastic character of the collision by classical trajectory Monte Carlo simulations.

In our experiments, the de Broglie wavelengths corresponding to the collision velocities are much shorter than the size of the Rydberg atoms as well as of the optical tweezers. Therefore, the experiment is expected to yield the cross section for a collision between two classical particles. (For more detailed discussion see section 5.)

For a scattering potential  $V(r) = C_6/r^6$ , the scattering angle can be approximated by [40]:

$$\theta \simeq \frac{15\pi C_6}{4mv^2b^6}, \quad (4)$$

where  $m$  is the atom mass,  $b$  is the impact parameter, and  $v$  is the collision velocity.  $b$  is varied by adjusting the position ( $x_A$ ) of the optical tweezer. Assuming atom  $B$  is initially at rest, the condition for recapture after the collision time  $\tau = t_2 - t_1$  is given by

$$v\tau \sin \frac{\theta}{2} < d_B, \quad (5)$$

where the width of tweezer,  $d_B \sim 0.8 \mu\text{m}$ , is much smaller than the propagation distance  $v\tau > 10 \mu\text{m}$ . Therefore, the atom  $B$  is recaptured after ‘soft’ collisions with small diffraction angles  $\theta < \theta_{\min} \simeq 2d_B/(v\tau)$ . The corresponding maximal impact parameter becomes

$$b_{\max} = \left( \frac{15\pi C_6 \tau}{8md_B v} \right)^{1/6}. \quad (6)$$

Consequently, the effective scattering cross section scales as:

$$\sigma_{\text{eff}} = \pi b_{\max}^2 \propto \left( \frac{C_6 \tau}{v} \right)^{1/3}. \quad (7)$$

Given the approximate  $n$  dependence of  $C_6 \propto n_{\text{eff}}^{11}$ , where  $n_{\text{eff}}$  is the effective quantum number for Rydberg atoms and the relation  $\tau \sim 1/v$  in this setup, the cross section scales as  $\sigma_{\text{eff}} \propto n_{\text{eff}}^{11/3} v^{-2/3}$ . More precisely, the numerical evaluation of  $C_6$  [37] is fitted by a scaling of  $C_6 \sim n_{\text{eff}}^{11.47}$  (see table 1 for values of  $C_6$ ,  $b_{\max}$ , and  $\sigma_{\text{eff}}$ ), which suggests the cross section scales as

$$\sigma \propto n_{\text{eff}}^{3.8} v^{-0.67}. \quad (8)$$

A Monte Carlo simulation has been performed to corroborate the above scaling analysis (see table 2 for values for the simulation). The electronic excitation of each atom by the laser field is treated as a two-level system and the atomic motion in terms of classical trajectories. The initial positions and the velocities of both atoms  $A$  and  $B$  at  $t=0$  (right after the tweezers are deactivated) are randomly generated based on the canonical thermal distribution of particles in the optical tweezer. Typically  $10^5$  pairs of initial conditions are used in the current study. After the tweezers are turned off, while the atoms move along straight-line trajectories, the electronic excitation is simulated with the Hamiltonian in the rotating wave approximation

$$H_e = \frac{1}{2} \Omega(\vec{r}, t) (|g\rangle\langle n| + |n\rangle\langle g|) \quad (9)$$

using the position dependent Rabi frequency (equation (1)) to calculate the excitation probability,  $\Gamma_{AB}$ . During the excitation phase, the atoms are sufficiently far apart so that van der

**Table 1.** Rydberg interaction constants [37], maximum impact parameter  $b_{\max}$ , and effective (classical) collisional cross section  $\sigma_{\text{eff}}$  (equation (7)) for two-body Rydberg–Rydberg scattering.

States	$C_6$ (GHz $\mu\text{m}^{-6}$ )	$b_{\max}$ ( $\mu\text{m}$ )		$\sigma_{\text{eff}}$ ( $\mu\text{m}^2$ )	
		$v_{\text{slow}}$	$v_{\text{fast}}$	$v_{\text{slow}}$	$v_{\text{fast}}$
$ 36S_{1/2}\rangle$	0.26	2.6	1.6	21.3	7.8
$ 45S_{1/2}\rangle$	4.23	4.1	2.5	54.1	19.7
$ 53S_{1/2}\rangle$	31.0	5.8	3.5	105.0	38.3

**Table 2.** Parameters used for numerical simulation.

$v$ ( $\text{m s}^{-2}$ )	$z_i$ ( $\mu\text{m}$ )	$t_f$ ( $\mu\text{s}$ )	$\Omega_0/(2\pi)$ (MHz)		
			$n=36$	$n=45$	$n=53$
0.85	10.0	33.3	1.06	0.84	0.92
3.0	14.1	8.2	1.09	0.88	0.94

Waals interactions can be neglected. For each random realization, a Monte Carlo method is used to determine whether the atoms are excited or not. If both atoms are excited, the collision dynamics are then simulated using the Hamiltonian

$$H = \frac{p_A^2}{2m} + \frac{p_B^2}{2m} + \frac{C_6}{|\vec{r}_A - \vec{r}_B|^6}. \quad (10)$$

If neither atom is excited, they continue on straight-line trajectories without interacting. The equations of motion for the atoms are numerically integrated using the Runge–Kutta method with adjustable time steps to properly account for the singularity of the van der Waals potential [35]. To obtain an accurate estimate for the electronic excitation dynamics between the two  $\pi$ -pulses we solve a Lindblad equation, which accounts for spontaneous decay and dephasing of the Rydberg state during this period [41]. In the current simulation the radiative lifetime of Rydberg states are approximated by  $t_n = 5 \times 10^{-4} n_{\text{eff}}^3$  yielding  $18 \mu\text{s}$  for  $n=36$ ,  $37 \mu\text{s}$  for  $n=45$ , and  $62 \mu\text{s}$  for  $n=53$ . The dephasing rate  $\gamma$  is set to  $1/\gamma = 150 \mu\text{s}$ . (Note that the simulations show that the final results are not sensitive to the value of  $\gamma$ .) Once one of the atoms decays to the ground state, the atoms follow straight-line trajectories. At  $t=t_2$ , the de-excitation probability via the second  $\pi$ -pulse is calculated only if atom  $B$  remains within the recapture zone. At the reactivation of the tweezer  $t=t_f$ , the recapture probability  $P_B$  is determined by counting how many random realizations result in the atom  $B$  remaining within the recapture zone and being de-excited to the ground state. To determine whether atom  $B$  remains in the trap upon reactivation, we approximate the optical tweezer by a sufficiently deep harmonic potential. Since the static tweezer depth  $U_s = 0.58(5) \text{mK}$  far exceeds the temperature of the stationary atom of about  $30 \mu\text{K}$ , this assumption simplifies the recapture condition to the requirement that the total kinetic energy does not exceed the trap depth. Hence, equation (5) remains a reliable approximation for the recapture process in our experiment.

To examine the effects of inelastic scattering, we have also performed another Monte Carlo simulation extending the

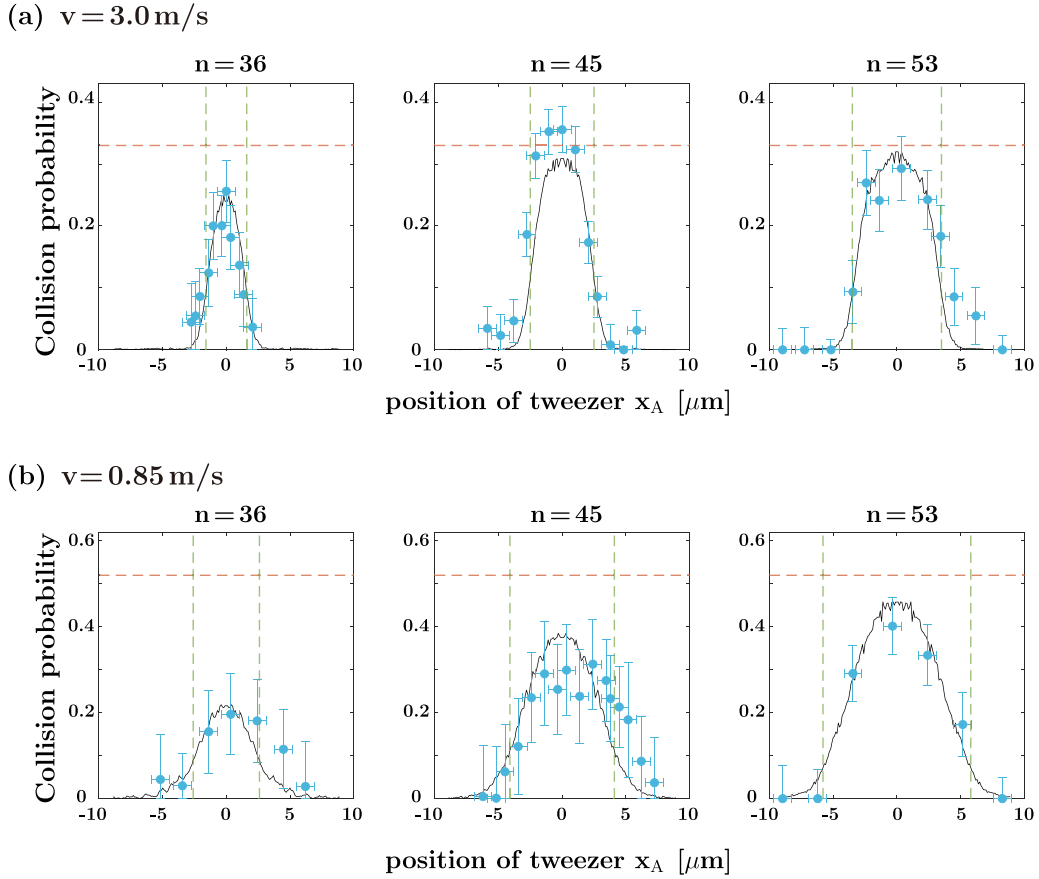


**Figure 2.** Measured (symbols) and calculated (solid lines) elastic collisional probabilities for Rydberg–Rydberg collisions with  $n = 36, 45,$  and  $53,$  at two different collision velocities:  $v = 3.0(2) \text{ m s}^{-2}$  (upper panel), and  $v = 0.85(9) \text{ m s}^{-2}$  (lower panel). Vertical dashed lines indicate  $b_{\text{max}}$  in table 1 below which scattering is expected ( $|x_A| < b_{\text{max}}$ ). Horizontal dashed lines indicate the photoexcitation probability  $\Gamma_{AB}$ . In the Monte Carlo simulations each data point represents an average over  $10^5$  random realizations.

above model. When both atoms are excited to the Rydberg state, a four-body system consisting of two Rydberg electrons and two  $\text{Rb}^+$  ion cores is simulated assuming both electrons and atoms follow the classical equations of motion. This simulation indicates that most inelastic processes are associated with large momentum transfers to the atom  $B$  for which the atom  $B$  will not be recaptured. Only for large  $n$  and  $v$ , a few inelastic processes allow for the recapture of the atom  $B$ . However, the probability of those inelastic processes is comparable or smaller than the error bars of the measurements. Therefore, those inelastic processes can be neglected in the current study.

#### 4. Experimental results

Experimental results for the impact parameter dependent collision probabilities  $P_{\text{coll}}(x_A = b; n, v)$  are presented in figure 2. They are determined via equations (2) and (3) for three different Rydberg states,  $|36S_{1/2}\rangle$ ,  $|45S_{1/2}\rangle$ , and  $|53S_{1/2}\rangle$ , and two collision velocities,  $v_{\text{fast}} = 3.0(2) \text{ m s}^{-2}$  and  $v_{\text{slow}} = 0.85(9) \text{ m s}^{-2}$ . The higher the Rydberg state ( $n$ ) of an atom and the slower the collision velocity ( $v$ ), the larger the position of the tweezer  $d = x_A$  at which collisions occur, as

expected from equation (7). The results are in a reasonable agreement with numerically simulated collision probabilities (solid lines).

The Monte Carlo simulation accounts for the impact parameter profiles of the two-body collisions in the current experiment. The position of the tweezer  $x_A$  serves as the representative of the impact parameter  $b$  of the two-body collision. When the actual impact parameter distribution is averaged over random realizations and compared to the value  $x_A$  (figure 3),  $x_A$  represents the average impact parameter for  $v = 3 \text{ m s}^{-2}$  reasonably well except at small  $x_A$ . However, for  $v = 0.85 \text{ m s}^{-2}$ , the thermal velocity spread ( $\sim 0.1 \text{ m s}^{-2}$ ) becomes comparable to the average velocity and the deviations become rather large. Overall,  $x_A$  tends to underestimate the average impact parameter. The Monte Carlo simulation also displays the effect of thermal diffusion which causes the atom  $B$  to escape the recapture zone and decreases the recapture probability,  $P_B(x_A; n, v)$ , even for large  $x_A$ , e.g.  $P_B(x_A; n, v_{\text{fast}}) \sim 0.56$ , and  $P_B(x_A; n, v_{\text{slow}}) \sim 0.01$ . These values correspond to the recapture probabilities without collision  $P_B^{(0)}(n, v)$ . For small  $x_A$  the two-body collision is expected to eject atom  $B$  only when both atoms  $A$  and  $B$  are excited to the Rydberg state and the van der Waals interaction becomes non-negligible. Therefore, the

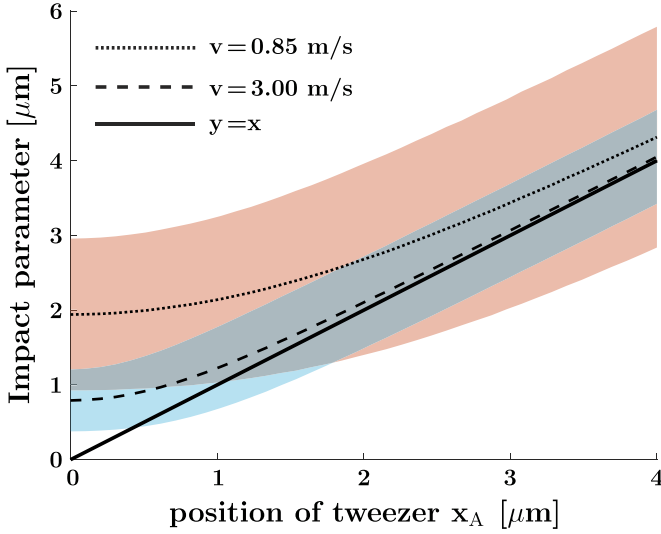


**Figure 3.** Average impact parameter as a function of  $x_A$  determined by Monte Carlo simulations evaluated over randomly generated positions and velocities of atoms  $A$  and  $B$  representing canonical ensembles in optical tweezers. For  $v = 3 \text{ m s}^{-2}$ ,  $x_A$  (dashed line) represents the average impact parameter well except at small  $x_A$  within a standard deviation (blue shaded). For  $v = 0.85 \text{ m s}^{-2}$  (dotted line), for which the thermal velocity spread ( $\sim 0.1 \text{ m s}^{-2}$ ) becomes comparable to the average velocity the deviations (red shaded) becomes rather large. For the atom  $A$  the trap frequency is  $294 \text{ kHz}$  and the temperature  $150 \mu\text{K}$  centered at  $\vec{r} = (x_A, 0, -z_i)$  and  $\vec{v} = (0, 0, v)$ . For the atom  $B$  the trap frequency is  $67 \text{ kHz}$  and the temperature  $30 \mu\text{K}$  centered at  $\vec{r} = (0, 0, 0)$  and  $\vec{v} = (0, 0, 0)$ .  $z_i = 10 \mu\text{m}$  for  $v = 0.85 \text{ m s}^{-2}$  and  $14.1 \mu\text{m}$  for  $v = 3 \text{ m s}^{-2}$ .

photoexcitation probability  $\Gamma_{AB}$  (horizontal dashed lines in figure 2) that both atoms,  $A$  and  $B$ , are excited by the first  $\pi$ -pulse serves as the upper bound of the collision probability at small  $x_A$ . Since the actual impact parameter  $b$  can be larger than  $x_A$  (figure 3), the atom  $B$  can be recaptured when  $b > b_{\text{max}}$  even for small  $x_A$  reducing the collision probability relative to  $\Gamma_{AB}$ . The spontaneous decay of Rydberg states is another factor to further reduce the collision probability. For  $n = 53$ , the lifetime of  $62 \mu\text{s}$  and  $b_{\text{max}}$  become large enough such that the collision probability in the limit of  $x_A \rightarrow 0$  nearly converges to the photoexcitation probability  $\Gamma_{AB}$ . The error introduced by the representation of the impact parameter  $b$  by the tweezer position  $x_A$  enters also the comparison between experimental and theoretical data for the differential collision probabilities (figure 2). In addition, residual differences may also indicate effects of residual misalignment between the static and the dynamic tweezers.

Experimental effective total cross sections,  $\sigma_{\text{eff,ex}}(n, v)$ , are obtained from the data for the effective collision probabilities  $P_{\text{coll}}(x_A; n, v)$  via

$$\sigma_{\text{eff,exp}}(n, v) = \frac{2\pi}{\Gamma_{AB}} \int dx_A x_A P_{\text{coll}}(x_A; n, v) \quad (11)$$

where we have renormalized the collision probabilities by the photoexcitation probabilities  $\Gamma_{AB}$ . The resulting  $\sigma_{\text{eff,exp}}(n, v)$  values in table 3 lie below the predicted ‘clean’ cross sections

**Table 3.** The cross-section  $\sigma_{\text{coll}}(n, v)$  of Rydberg-atom collisions (in unit of  $\mu\text{m}^2$ ).

States	$v = 0.85 \text{ m s}^{-2}$	$v = 3.0 \text{ m s}^{-2}$
$ 36S_{1/2}\rangle -  36S_{1/2}\rangle$	12.1	6.9
$ 45S_{1/2}\rangle -  45S_{1/2}\rangle$	31.4	16.7
$ 53S_{1/2}\rangle -  53S_{1/2}\rangle$	52.5	29.5

in table 1 for two-body collisions with well-defined velocity and impact parameter. We attribute this mainly to the deviation of  $x_A$  from the averaging over impact parameter, as shown in figure 3.

The numerical simulation can be further used to investigate the dependence of the effective collisional cross section on effective quantum number  $n_{\text{eff}}$  and collision velocity  $v$ . When the propagation distance between the two  $\pi$ -pulses is fixed to  $z_c = 16 \mu\text{m}$  and, correspondingly, the collision time,  $\tau = z_c/v$ , is inversely proportional to the collision velocity, the effective cross section is expected to follow the scaling  $\sigma_{\text{coll}} \propto n_{\text{eff}}^{3.8} v^{-0.67}$  (see equation (8)), as indicated in figure 4 by the dashed lines. This prediction can be compared with the simulation allowing for the thermal spread in velocity and position. The effective simulated cross section lies below the prediction for the ‘clean’ cross section as well.

For the dependence on the effective quantum number  $n_{\text{eff}}$  (figure 4(a)), the simulation yields  $\sigma \sim n_{\text{eff}}^{3.9}$  very close to the predicted scaling, while the collision velocity dependence in figure 4(b) is slightly off from the predicted scaling. We also attribute this primarily to the deviations of  $x_A$  from the effective impact parameter in figure 3. The deviations are most prominent for small collision velocities. As the velocity increases, the simulated results tend to converge towards the predicted cross sections.

## 5. Discussion

Within the context of cold collisions it is of conceptual interest to inquire into the regime of scattering angles at which quantum effects will become significant. We first note that the longitudinal de Broglie wavelength,  $\lambda_{\text{dB},\ell}$ , is much smaller than the size of the Rydberg atom ( $\langle r \rangle$ ), with values of  $1.5 \text{ nm}$  for  $v = 3 \text{ m s}^{-2}$  and  $5.4 \text{ nm}$  for  $v = 0.85 \text{ m s}^{-2}$ . More critical is therefore the ratio of the transverse de Broglie wavelength,  $\lambda_{\text{dB},t}$ , to the impact parameter  $b$ , which governs the collision process. This ratio,  $\lambda_{\text{dB},t}/b \ll 1$ , can be expressed as

$$p_t b \simeq \mu v \theta_{\text{qm}} b \simeq L \theta_{\text{qm}} \gg 1, \quad (12)$$

where  $\mu = m/2$  is the reduced mass and  $p_t$  is the transverse momentum. Replacing the classical angular momentum with the partial-wave quantum number,  $L = (l + 1/2)\hbar$ , equation (12) reduces to  $\ell \theta \gg 1 \simeq \ell \theta_{\text{qm}}$ . In the current case of rubidium Rydberg–Rydberg atom scattering, the characteristic impact parameters for elastic scattering at the asymptotic part of the van der Waals potential are larger than the atomic

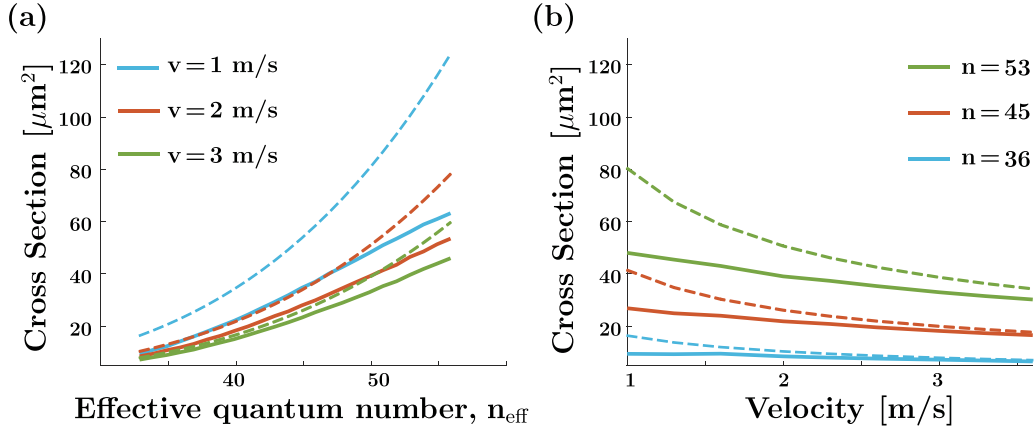


**Figure 4.** Simulated collisional cross section for a fixed propagation distance ( $8 \mu\text{m}$ ) between two  $\pi$ -pulses (solid lines) including thermal position and velocity spread. The initial position is set to  $z_i = 8 \mu\text{m} + v \times 1.5 \mu\text{s}$  and the Rabi frequency of  $\pi$ -pulses is 1 MHz. The total propagation time is  $t_f = 2z_i/v + 3 \mu\text{s}$ . (a)  $\sigma_{\text{coll}}$  as a function of  $n_{\text{eff}}$  and (b) as a function of  $v$ . The dashed lines are the predictions of equation (7) for ‘clean’ atom Rydberg–Rydberg scattering.

radius  $\langle r \rangle$ , i.e.  $b \gtrsim \langle r \rangle$ . Therefore, typical values of  $\ell$  are

$$\ell \simeq \mu v b \gg \mu v \langle r \rangle \simeq 100 \quad (13)$$

and are on the order of  $\sim 10^3$ . For all scattering angles, we find  $\theta_{\text{min}} \gg \theta_{\text{qm}} \simeq 10^{-3}$ , indicating that the (semi-)classical limit of quantum scattering applies. Therefore, the quantum scattering amplitude for scattering at the central potential  $V(r) = C_6/r^6$  (valid for  $r \gg \langle r \rangle$ ) can be evaluated in the (semi-)classical limit [38, 39]. The partial-wave scattering phase  $\delta_\ell$  for  $V(r)$  can be approximately given by [40],

$$\delta_\ell = -\frac{3\pi\mu^5 v^4 C_6}{16\ell^5}. \quad (14)$$

In the limit of large  $\ell$  the Legendre polynomials  $P_\ell$  become rapidly oscillating functions and the summation in scattering amplitude is dominated by the terms around the stationary phase  $\ell = L_0$  satisfying  $2 d\delta_\ell/d\ell|_{\ell=L_0} \pm \theta = 0$ . Thus, the scattering amplitude is approximated by [40]

$$f(\theta) \simeq \frac{1}{\mu v} \sqrt{\frac{L_0}{\sin\theta} \left| \frac{dL_0}{d\theta} \right|} e^{i(2\delta_{L_0} - (L_0 + 1/2)\theta - \pi/4)}. \quad (15)$$

Unlike the classical cross section  $\sigma_{\text{eff}}$  in equation (8), its quantum counterpart remains finite because of destructive quantum interferences between partial waves that are neglected in the classical limit. This cross section is given by

$$\sigma^{(\text{qm})} = 2\pi \int_0^\pi |f(\theta)|^2 \sin\theta d\theta \simeq \frac{8\pi}{\mu^2 v^2} \int_0^\infty L \sin^2 \delta_L dL. \quad (16)$$

For the scattering phases associated with the asymptotic part of van der Waals potential  $C_6/r^6$ , the quantum cross section follows the scaling law

$$\sigma^{(\text{qm})} \simeq 5.1 \left( \frac{C_6}{v} \right)^{2/5}. \quad (17)$$

Correspondingly, the effective cross section for the same constraint of hard collisions accessed by  $P_{\text{coll}}$  is given in terms of an upper cut-off for  $L_{\text{max}} = \mu v b_{\text{max}}$  by

$$\sigma_{\text{eff}}^{(\text{qm})} = \frac{8\pi}{\mu^2 v^2} \int_0^{L_{\text{max}}} L \sin^2 \delta_L dL. \quad (18)$$

Within the stationary-phase approximation, the scattering cross section becomes equivalent to the classical result

$$\frac{d\sigma}{db} = 2\pi \sin\theta |f(\theta)|^2 = 2\pi b \left| \frac{db}{d\theta} \right|. \quad (19)$$

Here  $b = \mu v L_0$ , and the scattering angle  $\theta$  follows from

$$\theta \simeq - \int_{r_0}^\infty \frac{2L_0}{r^2 \sqrt{2\mu(E - V(r)) - L_0^2/r^2}} dr + \pi, \quad (20)$$

where  $E = \mu v^2/2$  and  $r_0$  is the inner turning point, satisfying  $2\mu(E - V(r_0)) - L_0^2/r_0^2 = 0$ .

Figure 5 compares the quantum differential cross section (equation 19) evaluated using the scattering phase in equation (14), with the classical differential cross section (right-hand side of equation (19)) with  $f(\theta)$  calculated by expanding the integrand of equation (20) to first order in  $V(r)$ , i.e. using classical first-order perturbation theory for the long-range part of the van der Waals potential. The results show excellent agreement, except for the narrow forward cone ( $\theta \lesssim \theta_{\text{qm}}$ , see equation (12)), as expected. In the current experiment, with  $\theta_{\text{min}} > \theta_{\text{qm}}$ , classical two-body scattering is sufficient for analyzing the experimental data. However, making the experiment more sensitive to small scattering angles-by using smaller tweezers or lowering collision velocities-would render the Rydberg–Rydberg collision experiment sensitive to quantum scattering effects. For  $n = 36$  and  $v = 0.85 \text{ m s}^{-2}$  with a tweezer width of  $100 \text{ nm}$ ,  $\theta_{\text{min}} \simeq \theta_{\text{qm}}$  could be reached [42]. This would require an optical tweezer with a beam waist on the order of  $100 \text{ nm}$ , which is technically not feasible in the current experimental setup due to the diffraction limit on the order

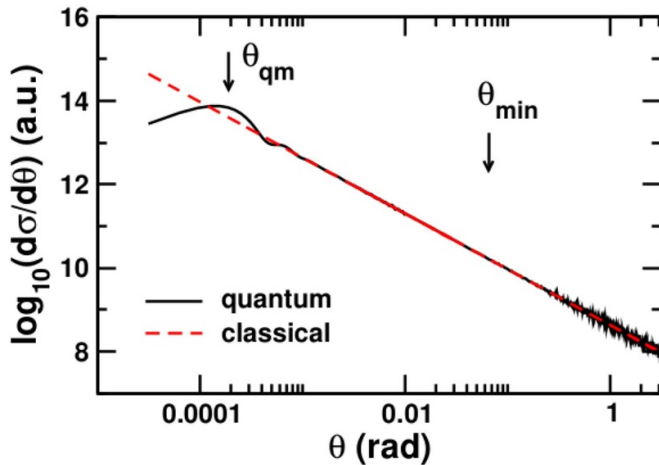


**Figure 5.** Comparison of classical and quantum differential cross sections,  $d\sigma/d\theta$ , for scattering between rubidium Rydberg–Rydberg atoms with the potential  $V(r) = C_6/r^6$ , at  $n = 36$  and  $v = 3 \text{ m s}^{-2}$ . The minimum scattering angle, which influences the effective scattering probability  $P_{\text{coll}}$  (equation (3)), is shown, along with the forward cone ( $\theta \leq \theta_{\text{qm}}$ ) where quantum effects become significant.

of optical wavelength. In order to implement optical tweezers with waists on that scale, a shorter wavelength optical tweezer would be required.

## 6. Conclusions

In summary, we have conducted an experiment of pairwise collisions of rubidium atoms in Rydberg energy states using optical tweezers. The initial positions and velocities of the atoms were controlled, allowing us to measure cross section profiles as a function of the effective impact parameter  $b$  and collision velocity  $v$  for selected Rydberg states  $|36S_{1/2}\rangle$ ,  $|45S_{1/2}\rangle$ , and  $|53S_{1/2}\rangle$ . By measuring the recapture probability, the acceleration of atom  $B$  induced by collision has been probed to extract the elastic scattering cross section without involving changes in the electronic excitation. The measured results were well reproduced by a numerical simulation that treats atomic motion classically and models the electronic excitation as a reduced two-level system, accounting for the thermal spread in position and velocity imposed by the optical tweezers. We have also delineated the parameter regime where the collision dynamics will be no longer fully classical but quantum effects become important.

## Data availability statement

The data cannot be made publicly available upon publication because no suitable repository exists for hosting data in this field of study. The data that support the findings of this study are available upon reasonable request from the authors.

## Acknowledgments

This work was supported by the National Research Foundation of Korea (NRF) Grant No. RS-2024-00340652, funded by the Korea government (MSIT) and by the Austrian science fund (FWF) Grant [10.55776/P35539]. For open access purposes, the author has applied a CC BY public copyright license to any author accepted manuscript version arising from this submission.

## ORCID iDs

Hansub Hwang  <https://orcid.org/0009-0000-5925-4230>  
 Sunhwa Hwang  <https://orcid.org/0000-0001-8945-0910>  
 Jaewook Ahn  <https://orcid.org/0000-0002-5837-6372>  
 Shuhei Yoshida  <https://orcid.org/0000-0002-6649-7692>  
 Joachim Burgdörfer  <https://orcid.org/0000-0002-1479-2657>

## References

- [1] Ashkin A, Dziedzic J M, Bjorkholm J E and Chu S 1986 Observation of a single-beam gradient force optical trap for dielectric particles *Opt. Lett.* **11** 288
- [2] Grimm R, Weidemüller M and Ovchinnikov Y B 2000 Optical dipole traps for neutral atoms *Adv. At. Mol. Opt. Phys.* **42** 95–170
- [3] Anderegg L, Cheuk L W, Bao Y, Burchesky S, Ketterle W, Ni K-K and Doyle J M 2019 An optical tweezer array of ultracold molecules *Science* **365** 1156
- [4] Svoboda K and Block S M 1994 Optical trapping of metallic Rayleigh particles *Opt. Lett.* **19** 930
- [5] Ashkin A, Dziedzic J M and Yamane T 1987 Optical trapping and manipulation of single cells using infrared laser beams *Nature* **330** 769
- [6] Kaufman A M and Ni K-K 2021 Quantum science with optical tweezer arrays of ultracold atoms and molecules *Nat. Phys.* **17** 1324
- [7] Brown M O, Muleady S R, Dworschack W J, Lewis-Swan R J, Rey A M, Romero-Isart O and Regal C A 2023 Time-of-flight quantum tomography of an atom in an optical tweezer *Nat. Phys.* **19** 569–73
- [8] Hwang H, Byun A, Park J, de Léséleuc S and Ahn J 2023 Optical tweezers throw and catch single atoms *Optica* **10** 401–6
- [9] Yoshida S, Burgdörfer J, Fields G, Brienza R and Dunning F B 2020 Giant cross sections for  $L$  changing in Rydberg–Rydberg collisions *Phys. Rev. A* **102** 022805
- [10] Olson R E 1979 Rydberg-atom–Rydberg-atom ionisation cross sections *J. Phys. B: Atom. Mol. Phys.* **12** L109
- [11] Matthies A J, Mortlock J M, McArd L A, Raghuram A P, Innes A D, Gregory P D, Bromley S L and Cornish S L 2024 Long-distance optical-conveyor-belt transport of ultracold  $^{133}\text{Cs}$  and  $^{87}\text{Rb}$  atoms *Phys. Rev. A* **109** 023321
- [12] Rakonjac A, Deb A B, Hoinka S, Hudson D, Sawyer B J and Kjærgaard N 2012 Laser based accelerator for ultracold atoms *Opt. Lett.* **37** 1085–7
- [13] Thomas R, Roberts K O, Tiesinga E, Wade A C J, Blakie P B, Deb A B and Kjærgaard N 2016 Multiple scattering dynamics of fermions at an isolated p-wave resonance *Nat. Commun.* **7** 12069

- [14] Horvath M, Thomas R, Tiesinga E, Deb A B and Kjergaard N 2017 Above-threshold scattering about a Feshbach resonance for ultracold atoms in an optical collider *Nat. Commun.* **8** 452
- [15] Thomas R, Chilcott M, Tiesinga E, Deb A B and Kjergaard N 2018 Observation of bound state self-interaction in a nano-eV atom collider *Nat. Commun.* **9** 4895
- [16] Krems R V 2008 Cold controlled chemistry *Phys. Chem. Chem. Phys.* **10** 4079
- [17] Khare S P 2001 Basics of collisions *Introduction to the Theory of Collisions of Electrons With Atoms and Molecules (Physics of Atoms and Molecules)* (Springer)
- [18] Tretyakov D B, Beterov I I, Yakshina E A, Entin V M, Ryabtsev I I, Cheinet P and Pillet P 2017 Observation of the borromean three-body Förster resonances for three interacting Rb Rydberg atoms *Phys. Rev. Lett.* **119** 173402
- [19] Härter A, Krülow A, Deiß M, Drews B, Tiemann E and Denschlag J H 2013 Population distribution of product states following three-body recombination in an ultracold atomic gas *Nat. Phys.* **9** 512–7
- [20] Fioretti A, Comparat D, Drag C, Gallagher T F and Pillet P 1999 Long-range forces between cold atoms *Phys. Rev. Lett.* **82** 1839
- [21] Zanon R A D S, Magalhaes K M F, de Oliveira A L and Marcassa L G 2002 Time-resolved study of energy-transfer collisions in a sample of cold rubidium atoms *Phys. Rev. A* **65** 023405
- [22] Walz-Flannigan A, Guest J R, Choi J-H and Raithel G 2004 Cold-Rydberg-gas dynamics *Phys. Rev. A* **69** 063405
- [23] Robicheaux F 2005 Ionization due to the interaction between two Rydberg atoms *J. Phys. B* **38** S333
- [24] Amthor T, Reetz-Lamour M, Westermann S, Denskat J and Weidemüller M 2007 Mechanical effect of van der Waals interactions observed in real time in an ultracold Rydberg gas *Phys. Rev. Lett.* **98** 023004
- [25] Niederprüm T, Thomas O, Manthey T, Weber T M and Ott H 2015 Giant cross section for molecular ion formation in ultracold Rydberg gases *Phys. Rev. Lett.* **115** 013003
- [26] Nagesha K and MacAdam K B 2003 Electron impact ionization of sodium Rydberg atoms below 2 eV *Phys. Rev. Lett.* **91** 113202
- [27] O’Keeffe P, Bolognesi P, Avaldi L, Moise A, Richter R, Mihajlov A A, Srećković V A and Ignjatović L M 2012 Experimental and theoretical study of the chemi-ionization in thermal collisions of Ne Rydberg atoms *Phys. Rev. A* **85** 052750
- [28] Zhelyazkova V and Hogan S D 2017 Electrically tuned Förster resonances in collisions of NH<sub>3</sub> with Rydberg He atoms *Phys. Rev. A* **95** 042710
- [29] Kim H, Lee W, Lee H, Jo H, Song Y and Ahn J 2016 In situ single-atom array synthesis using dynamic holographic optical tweezers *Nat. Commun.* **7** 13317
- [30] Lee W, Kim H and Ahn J 2016 Three-dimensional rearrangement of single atoms using actively controlled optical microtraps *Opt. Express* **24** 9816
- [31] Kim H, Park Y, Kim K, Sim H-S and Ahn J 2018 Detailed balance of thermalization dynamics in Rydberg-atom quantum simulators *Phys. Rev. Lett.* **120** 180502
- [32] Kim M, Song Y, Kim J and Ahn J 2020 Quantum Ising Hamiltonian programming in trio, quartet and sextet qubit systems *PRX Quantum* **1** 020323
- [33] Hwang S, Hwang H, Kim K, Byun A, Kim K, Jeong S, Soegianto M P and Ahn J 2025 Fast and reliable atom transport by optical tweezers *Opt. Quantum* **3** 64
- [34] Tüchendler C, Lance A M, Browaeys A, Sortais Y R P and Grangier P 2008 Energy distribution and cooling of a single atom in an optical tweezer *Phys. Rev. A* **78** 033425
- [35] Abrines R and Percival I C 1966 Classical theory of charge transfer and ionization of hydrogen atoms by protons *Proc. Phys. Soc.* **88** 861
- [36] Kim H, Kim M, Lee W and Ahn J 2019 Gerchberg-Saxton algorithm for fast and efficient atom rearrangement in optical tweezer traps *Opt. Express* **27** 2184
- [37] Robertson E J, Šibalić N, Potvliege R M and Jones M P A 2021 ARC 3.0: an expanded Python toolbox for atomic physics calculations *Comput. Phys. Commun.* **261** 107814
- [38] Berry M V and Mount K E 1972 Semiclassical approximations in wave mechanics *Rep. Prog. Phys.* **35** 315
- [39] Burgdörfer J, Reinhold C O, Sternberg J and Wang J 1995 Semiclassical theory of elastic electron-atom scattering *Phys. Rev. A* **51** 1248
- [40] Landau L D and Lifshitz E M 1977 *Quantum Mechanics Non-Relativistic Theory* 3rd edn, (Pergamon)
- [41] Meystre P and Sargent M 1998 *Elements of Quantum Optics* (Springer)
- [42] Romero M M, Alavi S K, Koistinen E M and Hong S 2023 Optomechanically induced optical trapping system based on photonic crystal cavities *Opt. Express* **31** 20398–409